Plasmonic properties of gold ring-disk nano-resonators: fine shape details matter

Nicolas Large,[1,2] Javier Aizpurua,[2] Vivian Kaixin Lin,[3] Siew Lang Teo,[3] Renaud Marty,[1] Sudhiranjan Tripathy,[3] and Adnen Mlayah[1,*]

[1]*Centre d'Elaboration de Matériaux et d'Etudes Structurales CEMES-CNRS, and Université de Toulouse, 29 rue Jeanne Marvig, BP 94347, 31055 Toulouse, France*
[2]*Centro Mixto de Física de Materiales CSIC-UPV/EHU, and Donostia International Physics Center (DIPC), Paseo Manuel de Lardizabal 5, 20018 San Sebastián, Spain*
[3]*Institute of Materials Research and Engineering (IMRE), A*STAR (Agency for Science, Technology and Research), 3 Research Link, 117602 Singapore*
[*]*adnen.mlayah@cemes.fr*

Abstract: Using numerical simulations, we demonstrate that fine shape details of gold nanoring-disks are responsible for significant modifications of their localized surface plasmon properties. The numerical results are supported by optical transmission measurements and by atomic force microscopy. In particular, we found that, depending on the ring wall sharpness, the spectral shift of the ring-like localized surface plasmon resonance can be as large as few hundred nanometers. These results shed the light on the strong sensitivity of the surface plasmon properties to very small deviations of the ring and disk shapes from the ideally flat surfaces and sharp edges. This effect is particularly important for tailoring the surface plasmon properties of metallic nanostrutures presenting edges and wedges for applications in bio- and chemical sensing and for enhancement of light scattering.

OCIS codes: (220.0220) Optical design and fabrication; (220.4241) Nanostructure fabrication; (160.4760) Optical properties; (240.6680) Surface plasmons.

References and links

1. A. J. Haes and R. P. Van Duyne, "A nanoscale optical biosensor: sensitivity and selectivity of an approach based on the localized surface plasmon resonance spectroscopy of triangular silver nanoparticles," J. Am. Chem. Soc. **124**, 10596–10604 (2002).
2. P. Alivisatos, "The use of nanocrystals in biological detection," Nat. Biotechnol. **22**, 47–52 (2004).
3. E. M. Larsson, J. Alegret, M. Käll, and D. S. Sutherland, "Sensing characteristics of NIR localized surface plasmon resonances in gold nanorings for application as ultrasensitive biosensors," Nano Lett. **7**(5), 1256–1263 (2007).
4. A. Dmitriev, C. Hägglund, S. Chen, H. Fredriksson, T. Pakizeh, M. Käll and D. S. Sutherland, "Enhanced nanoplasmonic optical sensors with reduced substrate effect," Nano Lett. **8**(11), 3893–3898 (2008).
5. J. Aizpurua, G. W. Bryant, L. J. Richter, F. J. García de Abajo, B. K. Kelley, and T. Mallouk, "Optical properties of coupled metallic nanorods for field-enhanced spectroscopy," Phys. Rev. B **71**, 235420 (2005).
6. F. Le, D. W. Brandl, Y. A. Urzhumov, H. Wang, J. Kundu, N. J. Halas, J. Aizpurua, and P. Nordlander, "Metallic nanoparticle arrays: a common substrate for both surface-enhanced Raman scattering and surface-enhanced infrared absorption," ACS Nano **2**, 707–718 (2008).
7. M. G. Banaee and K. B. Crozier, "Gold nanorings as substrates for surface-enhanced Raman scattering," Opt. Lett. **35**(5), 760–763 (2010).
8. S. Tripathy, R. Marty, V. K. Lin, S. L. Teo, E. Ye, A. Arbouet, L. Saviot, C. Girard, M. Y. Han, and A. Mlayah, "Acousto-plasmonic and eurface-4nhanced Raman ecattering properties of coupled gold nanospheres/nanodisk trimers," Nano Lett. **11**(2), 431–437 (2011).

#140906 - $15.00 USD Received 10 Jan 2011; revised 17 Feb 2011; accepted 27 Feb 2011; published 10 Mar 2011

9. K. Nakayama, K. Tanabe, and H. A. Atwater, "Plasmonic nanoparticle enhanced light absorption in GaAs solar cells," Appl. Phys. Lett. **93**, 121904 (2008).
10. M. A. Suarez, T. Grosjeana, D. Charrauta, and D. Courjon, "Nanoring as a magnetic or electric field sensitive nano-antenna for near-field optics applications," Opt. Commun. **270**(2), 447–454 (2007).
11. M. Schnell, A. García-Etxarri, A. J. Huber, K. Crozier, J. Aizpurua, and R. Hillenbrand, "Controlling the near-field oscillations of loaded plasmonic nanoantennas," Nat. Photonics **3**, 287–291 (2009).
12. N. Large, M. Abb, J. Aizpurua, and O. L. Muskens, "Photoconductively loaded plasmonic nanoantenna as building block for ultracompact optical switches," Nano Lett. **10**(5), 1741–1746 (2010).
13. S. A. Maier, *Plasmonics: Fundamentals and Applications* (Spinger-Verlag, 2007).
14. M. Pelton, J. Aizpurua, and G. Bryant, "Metal-nanoparticle plasmonics," Laser Photonics Rev. **2**, 1–24 (2008).
15. V. Giannini, A. I. Fernández-Domínguez, Y. Sonnefraud, T. Roschuk, R. Fernández-García, and S. A. Maier, "Controlling light localization and light-matter interactions with nanoplasmonics," Small **6**(22), 2498–2507 (2010).
16. L. C. Davis, "Electrostatic edge modes of a dielectric wedge," Phys. Rev. B **14**, 5523–5525 (1976).
17. S. Link, M. B. Mohamed, and M. A. El-Sayed, "Simulation of the optical absorption spectra of gold nanorods as a function of their aspect ratio and the effect of the medium dielectric constant," J. Phys. Chem. B **103**, 3073–3077 (1999).
18. M. I. Mishchenko, J. W. Hovenier, and L. D. Travis, *Light Scattering by Nonspherical Particles* (Academic Press, 2000).
19. C. Oubre and P. Nordlander, "Optical properties of metallodielectric nanostructures calculated using the finite difference time domain method," J. Phys. Chem B **108**, 17740–17747 (2004).
20. F. Hao, C. L. Nehl, J. H. Hafner, and P. Nordlander, "Plasmon resonances of a gold nanostar," Nano Lett. **7**(3), 729–732 (2007).
21. A. L. González and C. Noguez, "Influence of morphology on the optical properties of metal nanoparticles," J. Comput. Theor. Nanosci. **4**, 231–238 (2007).
22. N. Large, L. Saviot, J. Margueritat, J. Gonzalo, C. N. Afonso, A. Arbouet, P. Langot, A. Mlayah, and J. Aizpurua, "Acousto-plasmonic hot spots in metallic nano-objects," Nano Lett. **9**(11), 3732–3738 (2009).
23. B. N. Khlebtsov and N. G. Khlebtsov, "Multipole plasmons in metal nanorods: scaling properties and dependence on particle size, shape, orientation, and dielectric environment," J. Phys. Chem. C **11**, 11516–11527 (2007).
24. S. L. Teo, V. K. Lin, R. Marty, N. Large, E. Alarcon-Llado, A. Arbouet, C. Girard, J. Aizpurua, S. Tripathy, and A. Mlayah, "Gold nanoring trimers: a versatile structure for infrared sensing," Opt. Express **18**(21), 22271–22282 (2010).
25. P. Nordlander, "The ring: a leitmotif in plasmonics," ACS Nano **3**(3), 488–492 (2009).
26. J. Aizpurua, P. Hanarp, D. S. Sutherland, M. Käll, G. W. Bryant, and F. J. García de Abajo, "Optical properties of gold nanorings," Phys. Rev. Lett. **90**, 057401 (2003).
27. F. Hao, P. Nordlander, M. T. Burnett, and S. A. Maier, "Enhanced tunability and linewidth sharpening of plasmon resonances in hybridized metallic ring/disk nanocavities," Phys. Rev. B **76**, 245417 (2007).
28. F. Hao, Y. Sonnefraud, P. Van Dorpe, S. A. Maier, N. J. Halas, and P. Nordlander, "Symmetry breaking in plasmonic nanocavities: dubradiant LSPR sensing and tunable Fano resonance," Nano Lett. **8**(11), 3983–3988 (2008).
29. F. Hao, P. Nordlander, Y. Sonnefraud, P. Van Dorpe, and S. A. Maier, "Tunability of subradiant dipolar and Fano-type plasmon resonances in metallic ring/disk cavities: implications for nanoscale optical sensing," ACS Nano **3**(3), 643–652 (2009).
30. Y. Sonnefraud, N. Verellen, H. Sobhani, G. A. E. Vandenbosch, V. Moshchalkov, P. Van Dorpe, P. Nordlander, and S. Maier, "Experimental realization of subradiant, superradiant, and Fano resonances in ring/disk plasmonics nanocavities," ACS Nano **4**(3), 1664–1670 (2010).
31. Z. Ku and S. R. J. Brueck, "Experimental demonstration of sidewall angle induced bianisotropy in multiple layer negative index metamaterial," Appl. Phys. Lett. **94**, 153107 (2009).
32. V. Kaixin Lin, S. Lang Teo, R. Marty, A. Arbouet, C. Girard, E. Alarcon-Llado, S. Hua Liu, M. Yong Han, S. Tripathy, and A. Mlayah, "Dual wavelength sensing based on interacting gold nanodisk trimers," Nanotechnology **21**(30), 305501 (2010).
33. I. Romero, J. Aizpurua, G. W. Bryant, and F. J. García de Abajo, "Plasmons in nearly touching metallic nanoparticles: singular response in the limit of touching dimers," Opt. Express **14**, 9988–9999 (2006).
34. E. Prodan, C. Radloff, N. J. Halas, and P. Nordlander, "A hybridization model for the plasmon response of complex nanostructures," Science **302**, 419–422 (2003).
35. P. Nordlander, C. Oubre, E. Prodan, K. Li, and M. I. Stockman, "Plasmon hybridization in nanoparticle dimers," Nano Lett. **4**(5), 899–903 (2004).
36. Y. Wu and P. Nordlander, "Plasmon hybridization in nanoshells with a nonconcentric core," J. Chem. Phys. **125**, 124708 (2006).
37. F. J. García de Abajo and A. Howie, "Retarded field calculation of electron energy loss in inhomogeneous dielectrics," Phys. Rev. Lett. **80**, 115418 (1998).
38. F. J. García de Abajo and A. Howie, "Retarded field calculation of electron energy loss in inhomogeneous dielectrics," Phys. Rev. B **65**, 115418 (2002).
39. P. B. Johnson and R. W. Christy, "Optical constants of the noble metals," Phys. Rev. B **6**, 4370–4379 (1972).

#140906 - $15.00 USD Received 10 Jan 2011; revised 17 Feb 2011; accepted 27 Feb 2011; published 10 Mar 2011

40. W. J. Tropf, M. E. Thomas, and E. W. Rogala, *Handbook of Optics*, third ed., M. Bass, ed. (McGraw-Hill, 2010), Vol. 4, Chap. 2.
41. R. A. Paquin, *Handbook of Optics*, third ed., M. Bass, ed. (McGraw-Hill, 2010), Vol. 4, Chap. 4.

1. Introduction

Due to their optical properties, metallic nanoparticles and nanostructures are very interesting for various applications such as chemical and biological sensing [1–4], field-enhancement spectroscopies (SERS, SEIRA) [5–8], solar cells optimization [9], and highly integrated optical devices (resonators, optical emitters, nanoantennas, nanoswitches) [10–12]. The properties of metallic nanostructures include the optical excitation of surface plasmon resonances (LSPRs), strong localization of the energy at the nanometer scale, enhancement of electric fields, and resonance wavelength tunability [13–15]. The influence of morphology on the optical properties of small metallic nanoparticles has been studied both theoretically and experimentally by several groups [4, 14, 16–22]. Due to small defects, shape and size changes, strong variations in the optical properties of metallic nano-objects are expected and experimentally observed [23, 24].

Among the wide variety of plasmonic nano-resonators, ring-disks are very interesting nano-objects because they allow for a high tunability of the LSPR owing to the interaction between the nanoring walls [3, 7, 10, 25–28]. Moreover, it has been shown that small structural symmetry breaking of such nano-objects leads to strong variations of the LSPRs [28–30]. Nonzero sidewall angle effects have also been shown experimentally in metamaterials [31]. In this work, we investigate experimentally and numerically the dependence of the surface plasmon properties of ring-disks on fine shape details, namely the wall sharpness and profile of the nanoring and the nanodisk. The comparison between numerical and experimental results, combined with high-resolution scanning electron microscopy (HRSEM) and atomic force microscopy (AFM) images supports the importance of the fine shape details to fully determine optical properties of the ring-disks.

2. Nanofabrication and optical measurements

Two gold nanoring-disk samples NRD240 and NRD280, consisting in periodic arrays of concentric nanodisk (ND) and nanoring (NR), have been studied. The samples were fabricated using a protocol combining electron beam lithography (EBL) and thermal evaporation [8,24,32] of Au(25 nm)/Cr(3 nm) on quartz substrates. The ND and NR have a nominal height of $h = 28$ nm and were processed on a 100 μm x 100 μm area. Figure 1 shows HRSEM (a), AFM (b, d) images, and an AFM profile scan (c) of a typical nanoring-disk. The average size parameters extracted from the HRSEM and AFM measurements are quoted in Table 1. The axis to axis separation between ring-disks is 480 and 560 nm for samples NRD240 and NRD280, respectively. For such large separation, the electromagnetic nearfield interactions between adjacent ring-disks can be neglected [33].

The fine details of the shape of a typical ring-disk are revealed by the AFM measurements (Figures 1c and 1d). The fabrication process leads to two main features: i) the side walls of the NR and ND are not vertical but slightly tilted, ii) the NR and the ND do not present the ideal profile characterized by flat surfaces and sharp edges. They rather exhibit a rounded surface on top and smooth edges. Defects resembling small bumps and craters on the top of the ring-disk are also visible. One must keep in mind that the AFM resolution is limited by the tip size and by the response time of the experimental setup. The AFM image and topography profile in Figures 1d and 1c were acquired at low speed ($\tilde{v}_{tip} \approx 5$ μm/s) in order to reduce those limitations.

Figure 2 shows the optical density (OD) spectra of samples NRD240 and NRD280 obtained as $OD = -\log(T)$, where T is the measured transmittance. Spectra were recorded in the 400-

#140906 - $15.00 USD Received 10 Jan 2011; revised 17 Feb 2011; accepted 27 Feb 2011; published 10 Mar 2011

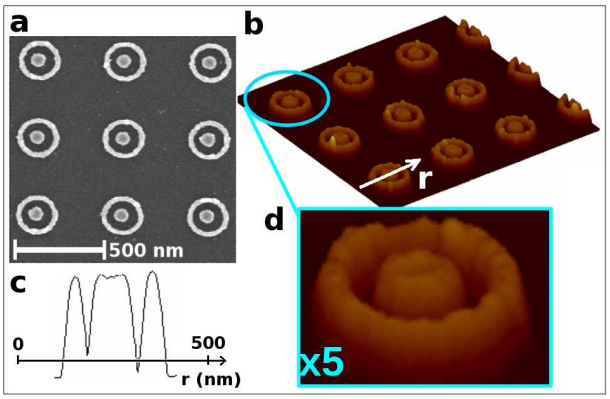

Fig. 1. HRSEM (a) and AFM (b, d) images of the NRD240 ring-disk sample. AFM profile scan (c) of a typical ring-disk.

Table 1. **Average size parameters from samples NRD240 and NRD280.** $D_{NR,out}$**,** $D_{NR,in}$ **and** w **are the outer and inner diameters and wall thickness of the NR, respectively.** D_{ND} **is the nanodisk diameter. The pitch, i.e. axis to axis separation between nanoring-disks, is also indicated.**

Samples	$D_{NR,out}$ (nm)	$D_{NR,in}$ (nm)	w (nm)	D_{ND} (nm)	Pitch (nm)
NRD240	240 $\pm$3	180 $\pm$3	30 $\pm$3	90 $\pm$3	480
NRD280	280 $\pm$3	202 $\pm$3	39 $\pm$3	112 $\pm$3	560

1700 nm spectral range and do not extend further into the infrared due to limitation of the spectrophotometer. The incident light was unpolarized. The transmitted light was collected through a 36X long working distance microscope objective with 0.5 numerical aperture. The probed area is around 250 μm^2 located at the center of the 100 μm x 100 μm processed area. The number of probed nano-objects is about 1100 and 800 in the case of ring-disks separated by 480 nm and 560 nm, respectively. As observed in Figure 2, the OD spectra exhibit two resonances: one in the visible (around 670 nm) and another in the infrared (around 1550 nm and 1700 nm depending on sample) which are associated to disk-like and ring-like LSPRs, respectively [27, 34–36]. The measured LSPR wavelengths and linewidths are quoted in Table 2. The ring-disks showed a good uniformity as attested by the weak dependence of the LSPR wavelengths on the probed point of the 100 μm x 100 μm area.

3. Simulations and comparison with experiments

To compare the experimental results with the calculations, we simulated the surface plasmon properties of ring-disks using the boundary elements method (BEM) [5, 26, 37, 38]. The bulk dielectric function of gold used in the calculations has been taken from Johnson and Christy [39]. Calculations were performed for a single ring-disk with characteristic dimensions corresponding to samples NRD240 and NRD280 (cf. Table 1). The ring-disk is located on the top of a quartz substrate (optical index from Ref. [40]), and the incident electric field $\vec{E}_i$ is propagating at normal incidence with polarization in the plane of the ring-disk. The 3 nm-Cr layer (optical index from Ref. [41]), that allows for improving the attachment of the ring-disk to the quartz substrate, is taken into account in the simulations.

The spectra presented in Figure 2 were calculated for a perfect ring-disk, i.e. for NR and ND

#140906 - $15.00 USD Received 10 Jan 2011; revised 17 Feb 2011; accepted 27 Feb 2011; published 10 Mar 2011

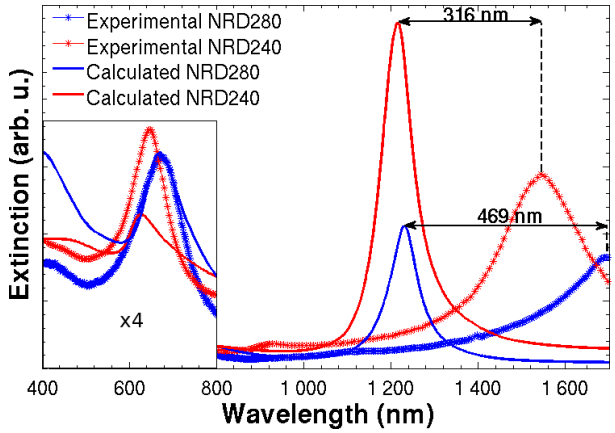

Fig. 2. Experimental (dots) and calculated (lines) spectra of the NRD240 (red) and NRD280 (blue) nanoring-disk samples. The BEM simulations assume perfect ring-disks with NR and ND showing flat surfaces and sharp edges. The scale in the range 400-800 nm is multiplied by a factor of 4.

with sharp edges and flat surfaces as sketched in (Figure 3a). The wavelength of the disk-like LSPR is correctly described by the calculations (see also Table 2). On the contrary, the discrepancy between measured and calculated wavelengths of the ring-like LSPR is considerable. Indeed, the ring-like LSPR measured for samples NRD240 and NRD280 are red-shifted by 316 nm and 469 nm, respectively, in comparison with the calculated LSPRs (Figure 2). Such differences cannot be explained by variations in the ND and NR sizes. Indeed, one needs to double the NR diameter in order to account for the measured ring-like LSPR wavelengths.

Since the ring walls are here very thin (30 nm and 39 nm for NRD240 and NRD280, respectively), their actual shape may strongly influence their surface plasmon resonances. In particular, the ring walls exhibit a rounded shape on top, rather than being ideally flat, as observed by AFM imaging and topography profiles (Figures 1d and 1c). Therefore, we study the influence of these fine shape details on the surface plasmon properties. Hence, we consider ring-disks with more realistic profiles, i.e. shapes mimicking those observed by AFM (Figure 3b). Instead of being vertical and sharp, the NR and ND walls are now tilted and have a rounded shape on top.

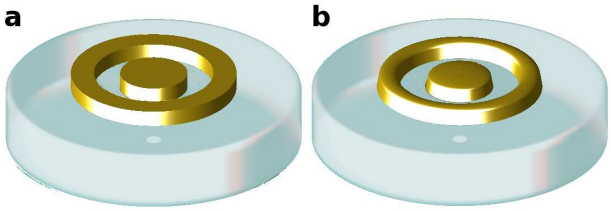

Fig. 3. Model profiles of ring-disks (a) with flat surfaces and sharp edges, and (b) with rounded surfaces and smooth edges.

Figure 4 presents extinction spectra of NRD240 and NRD280 ring-disks simulated for various ND and NR profiles. The disk-like LSPR λ_{ND} is only slightly affected by the change in shape: a maximum red-shift of only 11 nm with respect to the ideal sharp profile is found. Intuitively, this can be understood in terms of small shape deformation compared to the large disk size (either 90 nm or 112 nm in diameter). On the contrary, the infrared ring-like LSPR

#140906 - $15.00 USD Received 10 Jan 2011; revised 17 Feb 2011; accepted 27 Feb 2011; published 10 Mar 2011

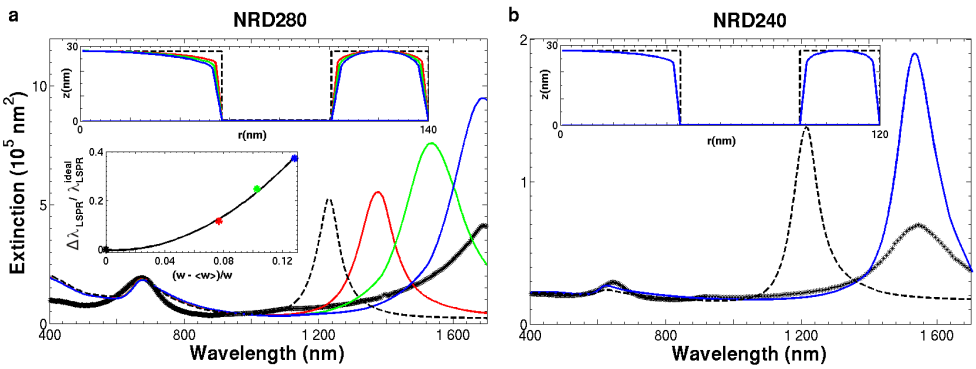

Fig. 4. Extinction spectra of NRD280 (a) and NRD240 (b) calculated for the various profiles of the ring-disks shown in the insets (only half the ring-disk is sketched). The spectrum corresponding to each profile is color-encoded. The profiles of the perfect ring-disks with sharp edges and flat surfaces and the corresponding spectra are shown in black dashed lines. The measured optical density spectra [$OD = -\log(T)$] are plotted with black dots. The inset in panel (a) shows the relative LSPR shift $\Delta\lambda/\lambda_{LSPR}^{ideal}$ as a function of the relative deviation of the mean NR wall thickness $(w - \langle w \rangle)/w$.

λ_{NR} red-shifts by several hundreds of nanometers with increasing deformation (Figure 4a). This significant spectral shift is directly connected to the interaction between inner and outer NR walls [26]. Indeed, by rounding the ring, both walls are slightly tilted and so result in a decrease of the mean wall thickness, thus leading to an increase of the inter-walls interaction. The smoother the edges are, the thinner the ring is, and the stronger the interaction becomes. This is the reason why the ring-like LSPR red-shifts when the rounded shape of the NR becomes more and more pronounced. The inset in Figure 4a shows the dependence of the relative spectral shift of the LSPR $\Delta\lambda/\lambda_{LSPR}^{ideal}$, λ_{LSPR}^{ideal} being the LSPR wavelength of the ideally flat ring-disk exhibiting sharp edges, as a function of the deviation of the mean NR wall thickness $\langle w \rangle$ from the nominal wall thickness w of the ideal NR. It can be noticed from this figure of merit that a 10% decrease of the mean wall thickness induces a 25% spectral red-shift of the ring-like LSPR. The strong sensitivity of the ring-like LSPR to small shape variations is due to the small ring wall thickness (either 30 nm or 39 nm). We specifically address this point further with the nearfield study. Figure 4b presents a comparison between the measured optical density (OD) spectrum and the extinction spectra simulated for both the ring-disk with sharp edges and the ring-disk with the rounded shape that accounts for the observed ring-like LSPR wavelength. This comparison is presented for sample NRD240 for which the infrared ring-like LSPR is clearly observed. The calculated LSPR wavelengths and linewidths are quoted in Table 2.

Table 2. **Calculated and measured LSPR wavelengths λ and linewidths Γ from the two ring-disk samples: NRD240 and NRD280. The accuracy of the wavelength determination is ± 2 nm.**

	NRD280				NRD240			
	λ_{ND} (nm)	Γ_{ND} (nm)	λ_{NR} (nm)	Γ_{NR} (nm)	λ_{ND} (nm)	Γ_{ND} (nm)	λ_{NR} (nm)	Γ_{NR} (nm)
Measured	676	115	~1700	~300	645	88	1546	223
Calculated	675	87	1688	210	630	61	1530	117

The experimental spectra are acquired from 1100 and 800 ring-disks in case of samples NRD240 and NRD280, respectively (cf. Section 2). The quantitative analysis of the ring-like

#140906 - $15.00 USD Received 10 Jan 2011; revised 17 Feb 2011; accepted 27 Feb 2011; published 10 Mar 2011

LSPR allows for determining the average shape of those probed ring-disks as shown in Figure 4. Furthermore, it is interesting to notice that the calculated ring-like LSPR is narrower and nearly three times more intense than the measured one (Table 2 and Figure 4b) in case of sample NRD240. We attribute this difference to the fact that the bulk dielectric function of gold is used in the simulations whereas our ring-disks present a high surface to volume ratio, which deviates from the bulk approximation. Moreover, size and shape fluctuations of the ring-disk as well as the roughness (bump and crater defects) visible in the AFM images (Figures 1b and 1d) have already been studied [19]. It has been shown that a distribution of about 360 bumps and craters with diameters ranging from 8 nm to 20 nm on the surface of a nanoshell induces a spectral red-shift of about 20 nm and contributes to the inhomogeneous broadening of the LSPR. The eccentricity of the ring-disks has also been studied both experimentally and theoretically [28–30]. A 17 nm displacement of the ND with respect to the NR center induces a spectral red-shift of the order of 25 nm. Considering the good quality of our samples, and the relatively small influence of the two effects (relative spectral shifts of the order of 2%), we can conclude that neither the presence of some defects (bumps and craters) nor the very small eccentricity of the ring-disks can be responsible for the significant spectral shift of the ring-like LSPR reported in our work.

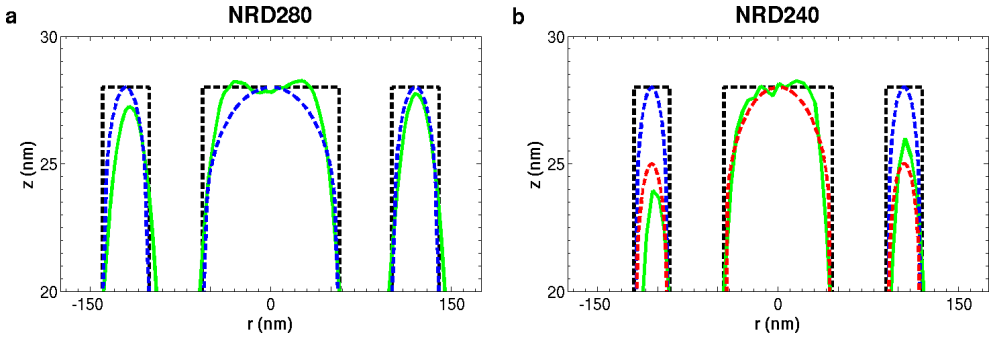

Fig. 5. Top part of the average AFM topography profiles (green lines) and of the model ring-disk profiles having both flat surfaces with sharp edges (black dashed lines), and rounded surface with smooth edges (blue dashed lines) for both samples NRD280 (a) and NRD240 (b). For NRD240, a profile with h_{NR} =25 nm< h_{ND} =28 nm is also shown in red dashed line.

Figure 5 compares the model profiles, extracted from the quantitative analysis of the extinction spectra (cf. Figure 3), to the top part of the AFM profiles (cf. Figure 1). The latter were obtained by averaging AFM-profile scans measured from 10 ring-disks of samples NRD240 and NRD280. The general feature of the realistic rounded ring-disk profiles is in good agreement with the measured topography profiles. In particular, the rounded shape of the NR top surface is well accounted for, though the actual AFM profiles appear broader due to experimental limitations, specially at the ring-disk base (cf. Section 2). However, the HRSEM image (cf. Figure 1c) shows a clear gap between the NR and the ND, thus supporting this AFM resolution limit. From the simulations, we found that a 3 nm broadening of the NR base (corresponding to the experimental accuracy) leads to a blue shift of the ring-like LSPR of about 15 nm. This value is much smaller than the shift induced by the rounded shapes (Figure 2). Furthermore, it can be noticed that for NRD240, the experimental NR height (h_{NR}) is slightly lower than that of the ND (h_{ND}). The calculations performed with a profile taking into account this mismatch (h_{NR} =25 nm< h_{ND} =28 nm, red dashed line in Figure 5b) show that the ring-like LSPR red-shifts by only 30 nm (with respect to the LSPR obtained with the ideal profile). Indeed, since the ring-like surface plasmon modes are related to the inter-walls interaction, the LSPRs only

#140906 - $15.00 USD Received 10 Jan 2011; revised 17 Feb 2011; accepted 27 Feb 2011; published 10 Mar 2011

weakly depend on the NR and ND height fluctuations.

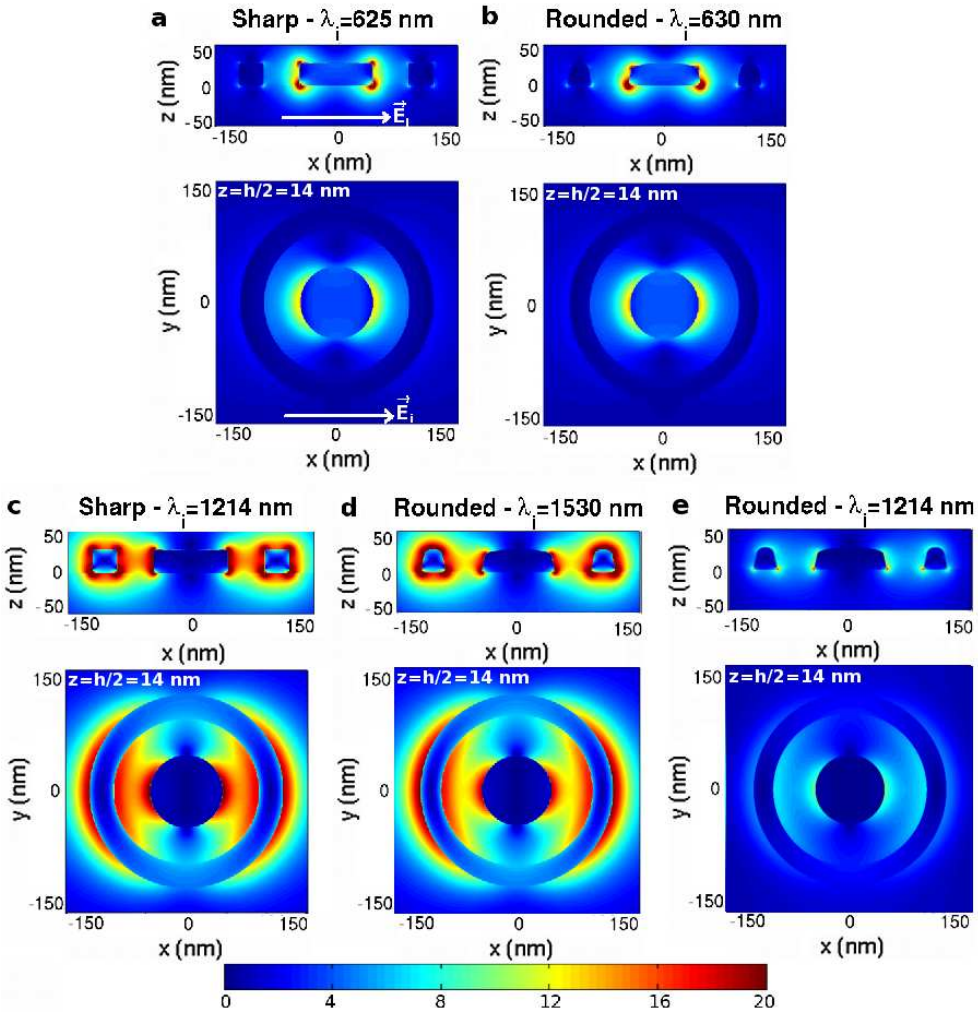

Fig. 6. All the upper panels show a side view at $y = 0$ and all the lower panels show a top view at $z = h/2 = 14$ nm of the calculated nearfield distributions for both sharp (a, c) and rounded (b, d) ring-disks (NRD240) associated to both disk-like (a, b) and ring-like (c, d) LSPRs. Panel (e) shows the nearfield distribution around the rounded ring-disk (NRD240) excited in resonance with the ring-like LSPR of the sharp ring-disk. The white arrow indicates the polarization of the incident field $\vec{E}_i$ which propagates along the z-direction. The color scale refers to the field enhancement factor $|\vec{E}_{loc}|/|\vec{E}_i|$.

It is interesting to determine the impact of the ring-disk shape on the surface plasmon nearfield distribution. To do so, we have calculated the local field enhancement $|\vec{E}_{loc}|/|\vec{E}_i|$ for both ring-disks with sharp edges and ring-disks with the rounded shape that accounts for the observed LSPRs (blue dashed line in Figure 5b). The results are presented in Figure 6 for the ring-disk NRD240. The nearfield distributions are shown for resonant excitation of the disk-like (Figures 6a and 6b) and ring-like (Figures 6c and 6d) LSPRs. For resonant excitation with the visible LSPR, only the dipolar surface plasmon mode of the ND is activated, thus supporting the

#140906 - $15.00 USD Received 10 Jan 2011; revised 17 Feb 2011; accepted 27 Feb 2011; published 10 Mar 2011

disk-like nature of this LSPR. Similarly, the resonant excitation of the infrared LSPR generates a strong field localization around the NR. This surface plasmon mode corresponds to the interaction between the NR walls. Moreover, part of the local field is also localized within the NR-ND gap due to the interaction between the NR and the ND. The spatial distributions of the nearfield intensity around the NR support the ring-like nature of the surface plasmon modes. Though slight amplitude changes can be noticed in Figures 6c and 6d, when rounding the NR and ND shapes, the general feature is preserved. These little changes arise from the sharpness of the NR edges. Indeed, in the sharp NR, there is a strong surface charge density localization on top of the NR sustained by the edges, while in the rounded NR it is quasi-uniformly distributed all over the NR wall. This effect reflects in the nearfield distribution (upper panels in Figures 6c and 6d). Furthermore, it is worthwhile to notice that the electric nearfield is more localized around the ring-disk with rounded surfaces and smooth edges (Figure 6d) due to stronger NR inter-walls interaction (as compared to Figure 6c). Figure 6e shows the nearfield distribution around the ring-disk with smooth edges and rounded surfaces with an incident wavelength in resonance with the LSPR of the ring-disk presenting sharp edges and flat surfaces ($\lambda_{LSPR}^{ideal} = 1214$ nm). From these nearfield maps we can notice that we are now out of resonance (lower local field enhancement) and that we loose the ring-like behavior (nearfield more localized within the NR-ND gap). Indeed, the LSP mode excited at 1214 nm is now the result of a mixing between the disk-like and the ring-like LSPRs.

4. Conclusion

Tailoring the optical properties of plasmonic nanostructures requires a complete understanding of the physical parameters that may influence the LSPR. Plasmonic nano-resonators are generally designed from numerical simulations of ideal nano-objects with the aim of targeting specific applications. In this work we showed that in a ring-disk, the ring-like LSPR wavelength is determined not only by the disk and ring diameters but also by the fine shape deformation of the ring walls and edges caused by the lithography and lift-off processes. We found that a rounded shape of the ring surfaces and edges is responsible for significant red-shifts of the ring-like LSPR that can be as large as 469 nm with respect to the perfect ring-disk with vertical side walls, flat surfaces and sharp edges. Moreover, based on numerical simulations and on a quantitative analysis of the shape effect we were able to extract, from the measured optical spectra, average ring-disk shapes. Good agreement was found with the AFM profiles. This work shows that the actual shape of plasmonic nano-resonators that exhibit small imperfections can strongly impact their LSPR properties. It sheds light on the importance of taking into account the fine shape details of nanostructures exhibiting corners, edges and wedges (e.g. bowtie antennas, nanorods, nanostars) and of systems involving strong electromagnetic interactions (e.g. sharp tip interacting with an object, coupled nanoantennas). This effect is also of importance for the accurate design of plasmonic structures for optical signal processing and control.

Acknowledgments

The authors thank funding supports from the French Embassy in Singapore under the MERLION Program, the Agency for Science, Technology and Research (A*STAR) in Singapore, from the European FP7 collaborative project “Nanoantenna” (Health-F5-2009-241818) and the project FIS2007-66711-C01-01 of the Spanish Ministry of Innovation and Science. The authors acknowledge the project inanoGUNE II from the ETORTEK project of the Department of Industry of the Basque Country.

#140906 - $15.00 USD Received 10 Jan 2011; revised 17 Feb 2011; accepted 27 Feb 2011; published 10 Mar 2011